Calculation of an axisymmetric turbulent wall jet over a surface of convex curvature

J. F. Morrison* and D. G. Gregory-Smith†

One of the many applications of curved wall jets of engineering importance is the Coanda Flare, which is used for burning waste gases in the petroleum industry and which gave rise to this work. The gas jet flows over an axisymmetric tulip shaped body, entraining ambient air and so promoting clean combustion. The object of this work was to calculate the development of the jet with the extra rates of strain imposed by both longitudinal curvature and divergence. A differential 'partially-parabolic' technique was used with uncoupling of the streamwise and cross-stream momentum equations, leading to an efficient computer program. The extra rates of strain were modelled by corrections to a mixing length model with the two effects being assumed to be additive. The calculation method was compared with seven test cases of experimental data. The first five were from published literature, and included the plane wall jet and axisymmetric free jet, and the separate effects of longitudinal curvature and divergence. The last two cases were measurements of the wall jet flow over a model Coanda Flare. The calculation method gave generally good results for the main features of the flow such as growth rate and velocity decay. Details of the flow were not so well predicted, particularly the turbulent shear stress, as a result of the relatively simple turbulence model employed. The calculation method should provide a useful engineering tool, but some profitable developments could be made, particulary in the area of turbulence modelling

Keywords: *fluid mechanics, gas flow, modelling, Coanda effect, flares*

Jets blown over convex surfaces will adhere to the surface, a phenomenon known as the Coanda effect. 'Destabilising' steamwise surface curvature increases turbulence in the jet, and so the entrainment of ambient fluid is increased. This property is used in the design of flares in the petroleum industry for burning waste gases, where the high entrainment promotes complete combustion. Such flares have been reported by Wilkins *et al*[1] and a typical geometry is shown in Fig 1. Higher pressure gas blows out radially from a slot at the base of the axisymmetric tulip shaped body and adheres to the surface entraining ambient air. Combustion is initiated near the top of the body, so that the flow around the lower part is largely uninfluenced by combustion. The design of these flares has been largely empirically based, and the aim of this work was to study the aerodynamics of the flare and to develop calculation techniques which could be used to improve future flare design.

This effect has been reported by several workers since the last century; Coanda patented a number of devices using the effect, and thus his name became associated with it (see Newman[2]). Bradshaw[3] distinguished three phenomena covered by the term 'Coanda effect': the tendency of a fluid to remain attached to a curved surface (an invisid effect), the tendency of jet placed near a surface to attach itself to the surface due to entrainment of ambient fluid (a viscous effect), and the effect of longitudinal curvature causing increased entrainment and jet growth. In the Coanda Flare, as well as the effect of longitudinal curvature, there is initially divergence of the flow at the base of the flare where the flow is radially outwards. This divergence is reduced as the flow goes round the surface until finally there is convergence on the conical top part of the flare. The longitudinal curvature and divergence/convergence of the flow were considered by Bradshaw[3] as extra rates of strain. Their effect on the turbulence structure is an order of magnitude

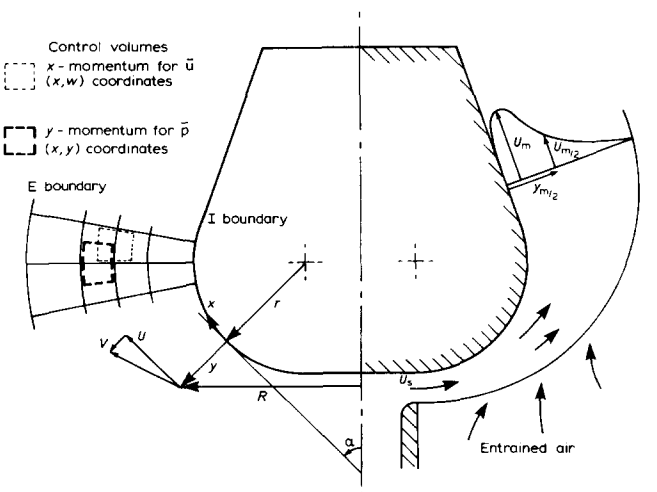

Fig 1 Coanda flare and co-ordinate system

* Department of Aeronautics, Imperial College, UK
† Department of Engineering, University of Durham, Science Laboratories, South Road, Durham, DH1 3LE, UK
Received 2 December 1983 and accepted for publication on 14 March 1984

greater than that suggested by the extra terms in the Reynolds stress transport equations.

For a wall jet on a flat surface, Glauert[4] produced a theoretical analysis, which was complemented by experimental work notably by Schwarz and Cosart[5] and Myers *et al.*[6] Wall jets over curved surfaces were studied by various workers including Guitton and Newman[7], Bradshaw and Gee[8], Alcaraz *et al.*[9] and Wilson and Goldstein[10]. They showed that the growth rate of the jet is greater than for a flat surface, with increased turbulent mixing in the outer part of the jet; the fluctuating component perpendicular to the surface is particularly increased. Below the velocity maximum, where the sign of the mean velocity gradient is positive, turbulent mixing is reduced, increasing the importance of turbulent diffusion from the outer to the inner region. In consequence, the position of zero shear stress, which is not coincident with the velocity maximum, moves towards the wall with increasing curvature.

Studies on the effects of divergence and convergence have been fewer. Bakke[11] studied the radial wall jet over a flat surface. On conical surfaces, Smits *et al*[12] studied the boundary layer flow and Sharma[13] investigated the wall jet. The extra rate of strain imposed by divergence gives greater growth rates than for a flat plate wall jet by up to 20% for a radial wall jet. Convergence gives the opposite effect.

Calculation of wall jet flows was based initially on integral methods, notably by Glauert[4], who matched a free jet outer part to a boundary layer inner part. The advent of computers has allowed the development of more powerful differential calculation techniques such as the 'Genmix' code developed by the group led by Spalding[14]. This is a general 'space marching' method for shear layer flows and can be applied to wall jets. Other differential methods have been developed, such as those by Bradshaw *et al*[15] and Cebeci and Smith[16]. All these methods require a turbulence model and, for this application, the model has to be modified for the effects of longitudinal curvature and divergence.

This paper discusses the development of a suitable turbulence model together with the associated calculation method. The results are compared with the measurements made on a model flare described in detail by Morrison[17].

Calculation method

Any shear layer calculation method requires that the grid is aligned approximately with the direction of flow. Thus in the method described below, shear layer axes are used initially. Large streamwise surface curvature implies the need for an iterative numerical scheme; transport equations are solved in finite difference form.

The coordinate system used to derive the equations of motion is shown in Fig 1. The x-direction follows the internal (I) boundary which can be either a solid surface of an axis of symmetry. I is a solid boundary in cases where $\partial p/\partial y \neq 0$ and the external (E) boundary is always the free edge of the shear layer. The grid is semi-curvilinear but orthogonal as shown in Fig 1. The flow will be referred to as 'plane' when the axisymmetric radius of curvature, R, tends to infinity. For a finite value of R, the flow is described as 'axisymmetric' and the control volume possesses both streamline and axisymmetric curvature.

For large streamline curvature where $\delta/r = O(0.1)$ an order of magnitude analysis of the equations of motion is necessary since neither the usual boundary layer approximation ($\partial p/\partial y = 0$) nor indeed the centrifugal approximation $\partial p/\partial y = \rho U^2/r$ is sufficient. It is assumed that $r/x = O(1)$, $V = O(U\delta/x)$, that $\sqrt{\overline{uv}}/U_m \sim 0.3$ and that other significant Reynolds stresses are of the same order. In general it may be supposed that gradients in the x- and y-directions will be of the same order as the dependent variable divided by x and δ respectively. h is approximated to unity. A consistent set of equations given by Bradshaw[3] is:

Notation

C_1, C_2 Constants, Eq (15)–(18)
e Extra strain rate
E External boundary
F Correction factor to mixing length (Eq (8))
h $1 + y/r$
I Internal boundary
K See Eq (20)
$k, \overline{q^2}/2$ Mean turbulent kinetic energy
l_c Corrected mixing length
l_0 Uncorrected mixing length
p Pressure
p' Fluctuating pressure
R Axisymmetric radius of curvature
r Longitudinal radius of curvature
Ri Richardson Number
Ri_B $= 2S(1+S)$ where $S = \dfrac{U/r}{\partial U/\partial y}$
t Slot height, time
U, V Mean velocities in x, y directions
u, v, w Fluctuating velocities in x, y, z directions
x Co-ordinate along surface, streamwise
y Co-ordinate perpendicular to surface
z Co-ordinate across surface (normal to x, y)
α Angle (Fig 1)
α, β Constants, Eqs (8) and (9)
α_1, α_2 Constants, Eq (20)
δ Jet thickness
ε Turbulent energy dissipation rate
θ Angle
κ, λ Mixing length constants
ν Kinematic viscosity
ψ Stream function
ρ Density
σ Constant, Eq (21)
ω Non-dimensional stream function
ξ $y/y_{m/2}$

Subscripts

m point at velocity maximum
m/2 point at half velocity maximum

x-momentum

$$U\frac{\partial U}{\partial x}+hV\frac{\partial U}{\partial y}+\frac{UV}{r}=\frac{1}{\rho}\frac{\partial p}{\partial x}-\frac{1}{R}\left\{\frac{\partial(\overline{u^2}R)}{\partial x}+\frac{\partial(\overline{huv}R)}{\partial y}+\frac{\overline{uv}R}{r}\right\}+\frac{v}{R}\frac{\partial}{\partial y}\left(Rh\frac{\partial U}{\partial y}\right) \quad (1)$$

y-momentum

$$-\frac{U^2}{r}=-\frac{h}{\rho}\frac{\partial p}{\partial y}-\frac{1}{R}\frac{\partial(\overline{hv^2}R)}{\partial y} \quad (2)$$

Continuity

$$\frac{\partial(UR)}{\partial x}+\frac{\partial(VRh)}{\partial y}=0 \quad (3)$$

retaining terms up to order δ/x only. In order that the approximations are consistent in both the x- and y-momentum equations, it should be noted that gradients in the y-momentum equation are x/δ times larger.

Eqs (1)–(3) are still elliptic despite the usual neglect of streamwise diffusion by viscosity. Only when $\partial p/\partial y=0$ and the pressure is a known function of x does the system of equations become parabolic. For cases reported below in which a parabolic system of equations is sufficient, the marching integration procedure of Patankar and Spalding[18] and Spalding[14] is used (PS method). A non-dimensional stream function:

$$\omega=\frac{\psi-\psi_x}{\psi_E-\psi_I} \quad (4)$$

is used as the cross-stream independent variable; transformation to (x,ω) coordinates renders the x-component momentum equation linear.

The differencing scheme uses upwind differences in the x direction and central differences in the y or ω direction giving a four-node implicit difference equation that is solved by a tri-diagonal matrix algorithm (tdma).

The calculation method has been extended to include an iterative scheme to permit solution of the full elliptic set of Eqs (1)–(3). It is similar to that of the 'partially-parabolic' scheme of Patankar and Spalding[19]. The algorithm sequence is:

1. The pressure field $p(x,y)$ is first guessed by assuming that $\partial p/\partial y=0$ and that the pressure is determined by the free steam pressure. For the cases reported here, the free stream pressure was always atmospheric.
2. The solution for U is available from the previous step. For the first step, (at the nozzle exit) U is calculated from the upstream stagnation pressure and the exit pressure distribution which is available from the previous iteration.
3. Eq (2) is integrated inwards from the free stream boundary to give the cross-stream pressure distribution.
4. Substitution of the continuity equation in Eq (1) via $\partial U/\partial x$ yields an ordinary differential equation in V.
5. The pressures at one grid location upstream from the present are adjusted by the difference between the newly calculated pressures and those from the previous iteration.
6. The x-momentum equation is solved in the (x,ω) coordinates but with the additional terms transformed and approximated in the same way.

Steps 2–6 are repeated until the whole flow domain has been covered. Iterations proceed until the wall static pressures change by no more than 0.2% of their absolute values. In practice convergence was accelerated by use of a relaxation factor of 0.3 applied to the pressure correction in Step 5. Fig 1 shows the control volumes used.

It should be noted that Eqs (1) and (2) are uncoupled by specifying $\partial p/\partial x$ as the gradient of the free stream, for this application, zero. Thus the solution for U is obtained effectively assuming $\partial p/\partial y=0$ while that for V uses values of pressure obtained from integration of Eq (2) and is stored as a two-dimensional array. In an elliptic system, mean flow transport and pressure disturbances proceed upstream at the rate of one x-step per iteration. Consistent with this, pressure corrections are applied at one grid location upstream. The algorithm is similar to that of Patankar and Spalding[19] although much simplified because for this application the y-momentum (Eq (2)) does not contain V. Thus V is obtained directly from the continuity equation and pressure corrections result only from the necessary uncoupling of the momentum equations rather than the additional non-satisfaction of the continuity equation. Patankar and Spalding use the Poisson equation to deduce pressure and velocity corrections.

The ordinary differential equation in V is solved by the second order Runge–Kutta approximation and the tdma with the coefficient for the $(i+1)$ node always zero (Fig 1). For cases in which the I boundary is a wall, Townsend's[20] modified law of the wall is used for near-wall grid and wall shear stress calculations. Values of $y_{m/2}$ and U_m are calculated using Newton's divided difference interpolating polynomial for three nodes.

The method is restricted to incompressible flow. Variable density of two mixing fluids is permitted, although only by simple mass average; scalar transport is not calculated. The use of upwind differences in the streamwise direction and also in the cross-stream direction, when there is large lateral flux by convection, make the numerical scheme unconditionally stable. The problem of numerical or 'false' diffusion is minimised by the use of streamline coordinates.

Turbulence modelling

The PS method has been applied to a wide variety of flow types with differing models, by Irwin and Smith[21], and Launder *et al*[22], amongst others. The current procedure can easily incorporate a full Reynolds stress closure. More recently, Gibson and Younis[23] have used a non-iterative version of the PS method with a Reynolds stress model for calculation of a curved wall jet with an extra rate of strain imposed only by streamline curvature. The ultimate aim of the present work is to apply the present calculation method with a Reynolds stress closure generally to flows with extra strain rates imposed by both axisymmetric and streamline curvature. For this purpose we apply a simplified model derived from the stress transport equations for $\overline{u^2}$, $\overline{v^2}$, $\overline{w^2}$ and $\overline{uv}$, which are, for high Reynolds numbers:

$$\frac{D(\overline{u^2}/2)}{Dt}=-\overline{u^2}\frac{\partial U}{\partial x}-\overline{huv}\frac{\partial U}{\partial y}-\frac{\overline{u^2}V+\overline{uv}U}{r} \quad \textit{PRODUCTION}$$

$$+\frac{\overline{p'\partial u}}{\rho\,\partial x} \quad \textit{REDISTRIBUTION}$$

$$-\frac{1}{\rho}\frac{\partial(\overline{p'u})}{\partial x}-\frac{3\overline{u^2v}}{2\ r}-\frac{1}{2R}\left(\frac{\partial(\overline{u^3}R)}{\partial x}+h\frac{\partial(\overline{u^2v}R)}{\partial y}\right)$$

TRANSPORT

$$-\frac{1}{3}\varepsilon$$

DESTRUCTION (4)

$$D\frac{(\overline{v^2}/2)}{Dt}=-\overline{uv}\frac{\partial V}{\partial x}-h\overline{v^2}\frac{\partial V}{\partial y}+2U\frac{\overline{uv}}{r}$$

PRODUCTION

$$+\frac{h}{\rho}\overline{p'\frac{\partial v}{\partial y}}$$

REDISTRIBUTION

$$-\frac{h}{\rho}\frac{\partial(\overline{p'v})}{\partial y}+\frac{\overline{u^2v}}{r}-\frac{\overline{v^3}}{2r}-\frac{1}{2R}\left(\frac{\partial(\overline{uv^2}R)}{\partial x}+h\frac{\partial(\overline{v^3}R)}{\partial y}\right)$$

TRANSPORT

$$-\frac{1}{3}\varepsilon$$

DESTRUCTION (5)

$$\frac{D(\overline{w^2}/2)}{Dt}=\frac{h}{\rho}\overline{p'\frac{\partial w}{\partial z}}$$

REDISTRIBUTION

$$-\frac{\overline{vw^2}}{2r}-\frac{1}{2R}\frac{\partial(\overline{uw^2}R)}{\partial x}+h\frac{\partial(\overline{vw^2}R)}{\partial y}$$

TRANSPORT

$$-\frac{1}{3}\varepsilon$$

DESTRUCTION (6)

$$\frac{D(-\overline{uv})}{Dt}=\overline{u^2}\left(\frac{\partial V}{\partial x}-\frac{U}{r}\right)+h\overline{v^2}\frac{\partial U}{\partial y}-\frac{U}{r}(\overline{u^2}-\overline{v^2})$$

$$-h\frac{\overline{uv}}{R}(U\sin\alpha+V\cos\alpha)$$

PRODUCTION

$$-\overline{\frac{p'}{\rho}\left(\frac{\partial v}{\partial x}+h\frac{\partial u}{\partial y}\right)}$$

REDISTRIBUTION

$$+\frac{\partial}{\partial x}\frac{(\overline{p'v})}{\rho}+\frac{1}{R}\frac{\partial(\overline{u^2v}R)}{\partial x}+\frac{h}{\rho}\frac{\partial(\overline{p'u})}{\partial y}+\frac{h}{R}\frac{\partial(\overline{uv^2}R)}{\partial y}$$

$$+\frac{2(\overline{uv^2}-\overline{u^3})}{r}$$

TRANSPORT (7)

Note that in addition to the implicit changes to these equations caused by higher order correlations, (Bradshaw[3]), the explicit changes introduced by the axisymmetric curvature give additional transport terms as well as an extra production term in Eq (7).

Now the simplified model is developed by:

(a) Approximating the transport equations leaving only the pressure-strain terms to be modelled.
(b) Modelling these terms following Launder *et al.*[22]
(c) Neglecting the production term introduced by divergence in Eq (7).
(d) Deriving the algebraic expressions for the effects of streamline curvature and divergence separately and assuming that they are linearly additive.

The procedure (a) and (b) for streamline curvature has been followed by Irwin and Smith[21] and So and Mellor[24], and amounts to a second order mixing length model. It is not expected that this modelling procedure will be of great accuracy except for mean flow predictions. The justification for the assumption of linearly additive effects of two rates of strain is simply that the crudity of the initial assumptions requires no more. This procedure does, however, provide the first view of the problem of modelling flows with two extra rates of strain.

Bradshaw[3] uses the local equilibrium approximation to develop a first order correction for the effects of small extra strain rates on thin shear layers of the form:

$$F=1+\alpha\frac{e}{\partial U/\partial y} \tag{8}$$

where α is of order 10. For streamline curvature an equivalent expression can be derived by analogy with the effect of buoyancy:

$$l_c/l_o=1-\beta Ri_B \tag{9}$$

where Ri_B is the flux Richardson number as defined by Bradshaw[25]. For large curvature, So and Mellor[24] and Irwin and Smith[21] have made less drastic assumptions than that of local equilibrium. Assuming that terms $\overline{u_iu_j}$ are of order $U^2(y_{m/2}/x)$, that terms $\overline{u_iu_ju_k}$ are of order $(y_{m/2}/x)^2\ U^3$, and that the redistribution terms are of the same order as the main production terms, Eqs (4)–(7) reduce to their local equilibrium form but with the pressure-strain terms retained. They are:

$$-h\overline{uv}\frac{\partial U}{\partial y}-U\frac{\overline{uv}}{r}+\overline{\frac{p'}{\rho}\frac{\partial u}{\partial x}}-\frac{1}{3}\varepsilon=0 \tag{10}$$

$$2U\frac{\overline{uv}}{r}+\frac{h}{\rho}\overline{p'\frac{\partial v}{\partial y}}-\frac{1}{3}\varepsilon=0 \tag{11}$$

$$\frac{h}{\rho}\overline{p'\frac{\partial w}{\partial z}}-\frac{1}{3}\varepsilon=0 \tag{12}$$

$$h\overline{v^2}\frac{\partial U}{\partial y}-(2\overline{u^2}-\overline{v^2})\frac{U}{r}-h\frac{\overline{uv}}{R}(U\sin\alpha+V\cos\alpha)$$

$$-\overline{\frac{p'}{\rho}\left(\frac{\partial v}{\partial x}+h\frac{\partial u}{\partial y}\right)}=0 \tag{13}$$

Also the turbulent energy equation becomes:

$$-h\overline{uv}\frac{\partial U}{\partial y}+U\frac{\overline{uv}}{r}-\varepsilon=0 \tag{14}$$

The pressure-strain terms are modelled as they were by Launder *et al*[22]. The two contributions, the first representing interactions of the turbulence and the second caused by the mean rate of strain effect on the turbulence, are added. The modelled equations are:

$$h\overline{uv}\frac{\partial U}{\partial y}+U\frac{\overline{uv}}{r}+C_1\varepsilon\left(\frac{\overline{u^2}}{q^2}-\frac{1}{3}\right)+$$

$$C_2\left(-\frac{2}{3}h\,\overline{uv}\frac{\partial U}{\partial y}-\frac{4}{3}\overline{uv}\frac{U}{r}\right)+\frac{\varepsilon}{3}=0 \qquad (15)$$

$$2U\frac{\overline{uv}}{r}+C_1\varepsilon\left(\frac{v^2}{q^2}-\frac{1}{3}\right)+C_2\left(\frac{1}{3}h\,\overline{uv}\frac{\partial U}{\partial y}+\frac{5}{3}U\,\frac{\overline{uv}}{r}\right)+\frac{\varepsilon}{3}=0 \qquad (16)$$

$$C_1\varepsilon\left(\frac{w^2}{q^2}-\frac{1}{3}\right)+C_2\left(\frac{1}{3}h\,\overline{uv}\frac{\partial U}{\partial y}-\frac{1}{3}U\frac{\overline{uv}}{r}\right)+\frac{\varepsilon}{3}=0 \qquad (17)$$

$$h\overline{v^2}\frac{\partial U}{\partial y}-(2\overline{u^2}-\overline{v^2})\frac{U}{r}+C_1\varepsilon\frac{\overline{uv}}{k}+$$

$$C_2\left(-h\overline{v^2}\frac{\partial U}{\partial y}+(2\overline{u^2}-\overline{v^2})\frac{U}{r}\right)-h\frac{\overline{uv}}{R}(U\sin\alpha+V\cos\alpha)=0 \qquad (18)$$

$$h\,\overline{uv}\frac{\partial U}{\partial y}-\overline{uv}\frac{U}{r}+\varepsilon=0 \qquad (19)$$

Launder *et al* use $C_1=1.5$ and $C_2=0.4$. No adjustments are made to the pressure-strain terms for near-wall turbulence. Manipulation of these five equations (without the divegence term in Eq (18)) yields an equation of the form:

$$-\overline{uv}=l_0^2(1-\alpha_1 Ri-\alpha_2 Ri^2)^{3/2}(1-K)^2\left(\frac{\partial U}{\partial y}\right)^2 \qquad (20)$$

where:

$$K=\frac{U/rh}{\partial U/\partial y}$$

and:

$$Ri=\frac{2K(1+K)}{(1-K)^2}$$

This procedure has been followed by So[26], Irwin and Smith[21] and So and Mellor[24]. The constants α_1 and α_2 are not universal, nor are their values a direct result of the constants used in the pressure-strain model: the modelling of the pressure-strain terms merely shows the correct functional form of the second order mixing length expression. The constants are geometry-dependent since they have to account for the neglect of the transport terms which are significant to a different degree, and for the neglect of wall influence on the pressure-strain model. For the cases considered below, however, they were taken as constants even though the effects of streamline curvature on turbulent transport are known to be large. Doubtless, better predictions could have been obtained by 'tuning' of these constants, although this would have been no more than a 'second order' refinement.

The effects of divergence are modelled in the form of Eq (8) where:

$$l_c=l_o\left[1-\sigma\frac{(U\sin\alpha+V\cos\alpha)}{R\,\partial U/\partial Y}\right] \qquad (21)$$

and the extra rate of strain is that which appears as an extra production term in Eq (7). The empirical constant σ is subject to the same arguments as above. Both Eqs (20) and (21) give the changes in mixing length expected with the extra strain rates.

The mixing length for plane wall jet cases, without divergence l_0, is calculated by separation of the jet into 'mixing regions' as in Fig 2 where standard values of $\kappa=0.41$ and $\lambda=0.09$ ($\lambda=0.075$ in the case of the round free jet) are used. Zero shear stress at a velocity maximum in the region y_2-y_3 was avoided by using values from the adjacent mixing regions, subject to a specified minimum. No allowance was made for history effects, ie changes in terms in the transport equations which do not occur immediately the mean rate of strain changes. However, any time constants associated with the time response of a shear layer to a sudden change in surface curvature are likely to be small in the present cases[3]. Eqs (1)–(3) are of course invalid where dR/dx or dr/dx is large.

Comparison with experiments

The calculation method was tested against experimental data for five independent cases, all of differing geometries (Table 1). The method was then used to predict the flow over the flare geometry for two different conditions, and the results compared with the measurements reported by Morrison[17].

Cases 5, 6 and 7 required the partially parabolic procedure, using the iteration for cross stream pressure gradient. No iteration was required for Cases 1–4. Case 3 is the only one with the I boundary as an axis of symmetry. For all cases the flow was effectively incompressible with the Mach Number less than 0.3. With the exception of the node adjacent to the wall, the nodes were distributed

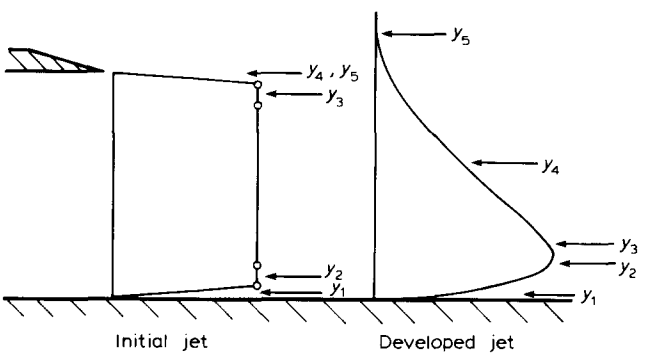

Fig 2 Mixing region boundaries

Table 1 Testcases

Case	Slot Reynolds number	Geometry
1	1.4 x 10^4	Flat-plate wall jet. Wilson and Goldstein[10] and Myers *et al*[6]
2	1.6 x 10^4	Radial flat wall jet. Bakke[11]
3	4.3 x 10^4	Round free jet. Rodi[27]
4	0.6 x 10^4	Conical wall jet. Sharma[13]
5	1.5 x 10^4	Wall jet over cylinder, Wilson and Goldstein[10]. r/t = 16.5
6	2.2 x 10^4	Flare geometry A. Morrison[17]. r/t = 6.0
7	1.4 x 10^4	Flare geometry B. Morrison[17]. r/t = 15.0

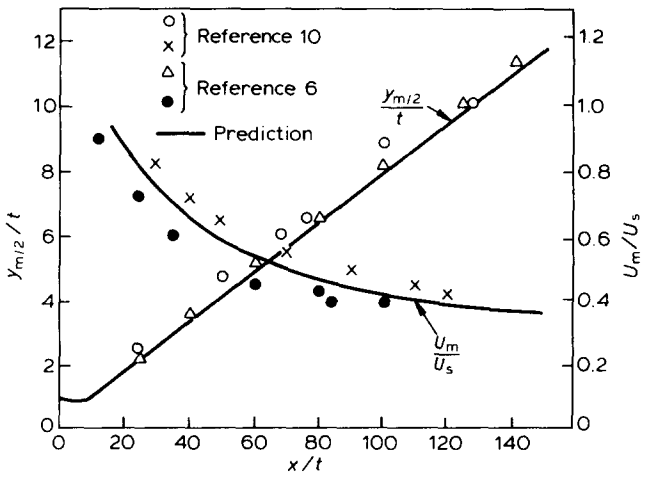

Fig 3 Case 1: growth/velocity decay

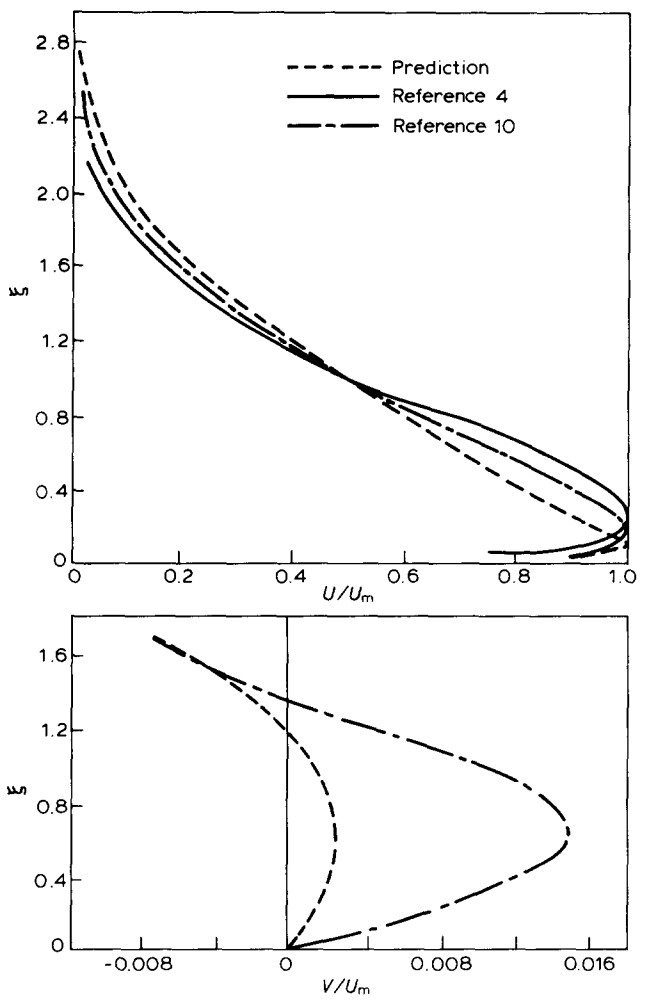

Fig 4 Case 1: mean velocity profiles

according to a power law of 1.5, so that the nodes were closer together near the maximum of the mean velocity profile.

Cases 1–5

The experimental data of Case 1 was used to fix the entrainment constants, which were subsequently not changed for the other cases. Fig 3 shows the growth rate and maximum velocity decay for the flat wall jet (Case 1) indicating the good agreement achieved by adjusting the entrainment constants. The mean velocity profiles are shown in Fig 4. The calculated streamwise profile has a peak which is sharper and closer to the wall than the measured profile, and the maximum normal velocity is seriously underestimated. These features are common to all the prediction cases. The shear stress profiles are shown in Fig 5, which shows the change of sign of shear stress near the wall. The agreement is generally good except near the outer part of the jet.

For Case 2, the radial wall jet, the growth rate and maximum velocity decay show satisfactory agreement (Fig 6). A value of $\sigma = 9.0$ was used in Eq (21) to account for the effect of streamline divergence on the mixing length. There was no experimental data for the shear stress, but Fig 7 shows the predicted shear stress about twice those for Case 1 (Fig 5) as expected.

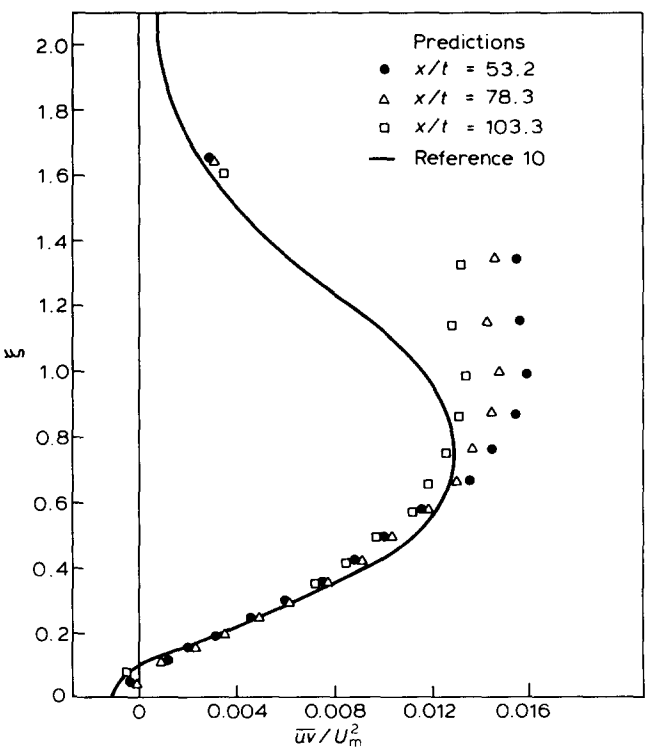

Fig 5 Case 1: shear stress profiles

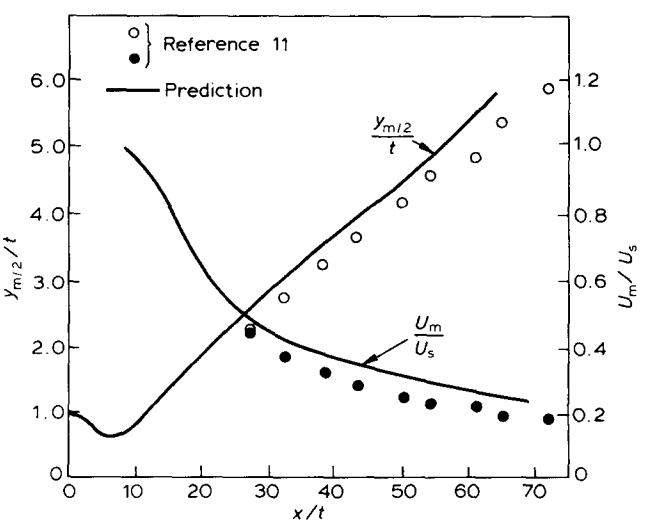

Fig 6 Case 2: growth/velocity decay

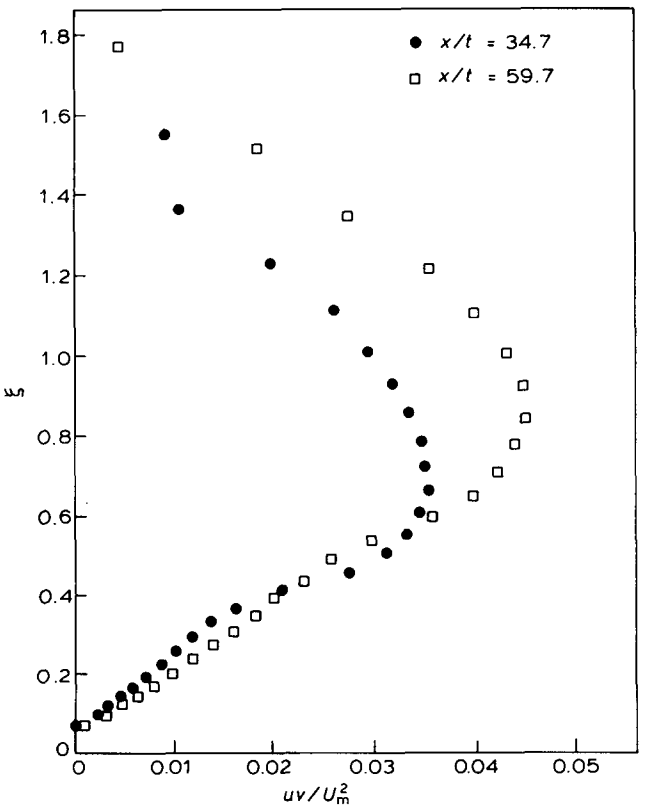

Fig 7 Case 2: shear stress profiles

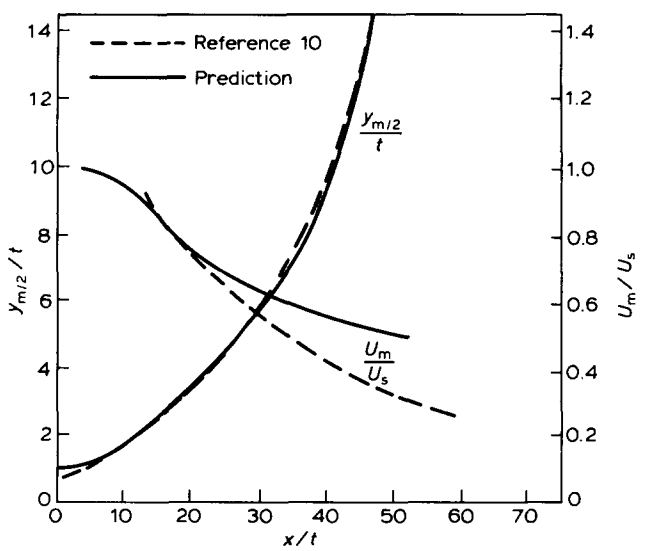

Fig 8 Case 5: growth/velocity decay

For Case 3, the round free jet, and Case 4, the conical wall jet, again satisfactory agreement was obtained for the growth rate and maximum velocity decay, with poorer agreement for mean velocity and shear stress profiles.

Case 5 was used to fix the two constants required for the correction to the mixing length for the effects of longitudinal curvature. It was found that the values suggested by So[24] were satisfactory, ie $\alpha_1 = 3.26$ and $\alpha_2 = 3.09$ in Eq (20). These values were not altered for the predictions for the flare geometry. The growth rate is predicted well, but the maximum velocity decay is not so well predicted (Fig 8). The shear stress profiles, Fig 9, are predicted with the right trend, but are not accurate in detail. For instance, the prediction at 90° peaks a little less than that for 120°, whereas the experiments indicate smaller values with the 130° results being lower than those at 90°. However, comparing with Fig 5 for the flat wall jet (Case 1) both the predicted and the experimental shear stress are much increased due to the longitudinal curvature.

Flare geometry, Cases 6 and 7

Cases 6 and 7 differ only in the slot height and velocity. The jet growth for Case 6 is shown in Fig 10. The initial reduction in thickness is due to the radial outflow close to the slot. The growth rate is predicted fairly well when compared with the experimental data from both a three-hole cobra probe and hot wire anemometry. Fig 10 also

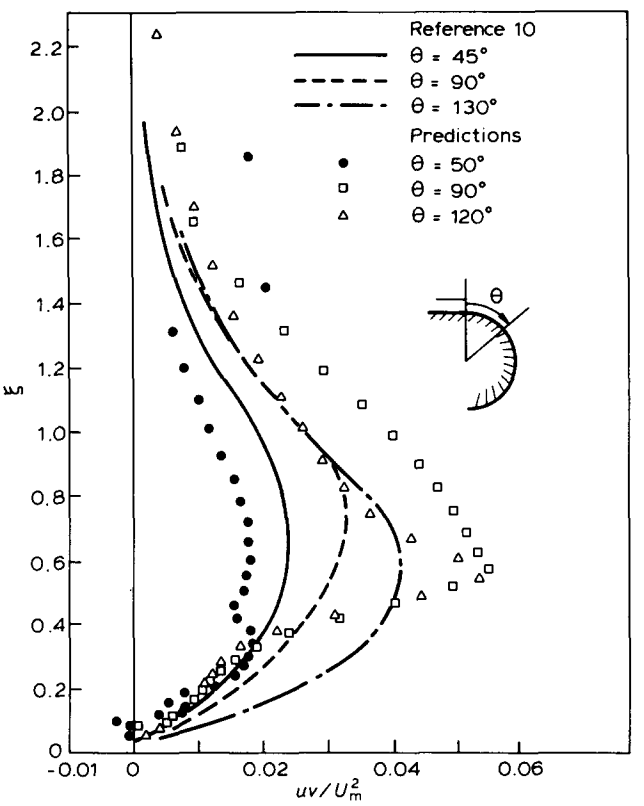

Fig 9 Case 5: shear stress profiles

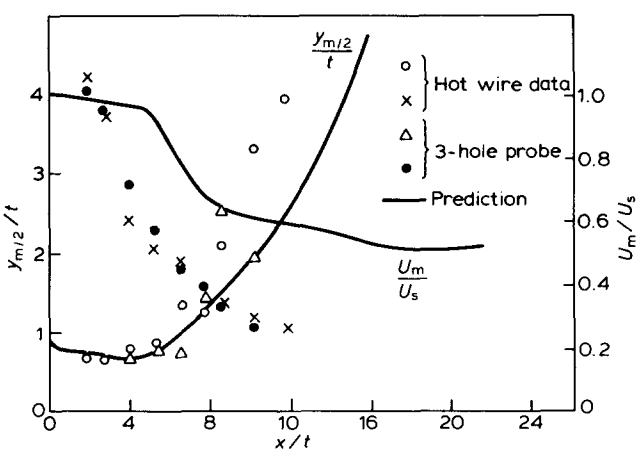

Fig 10 Case 6: growth/velocity decay

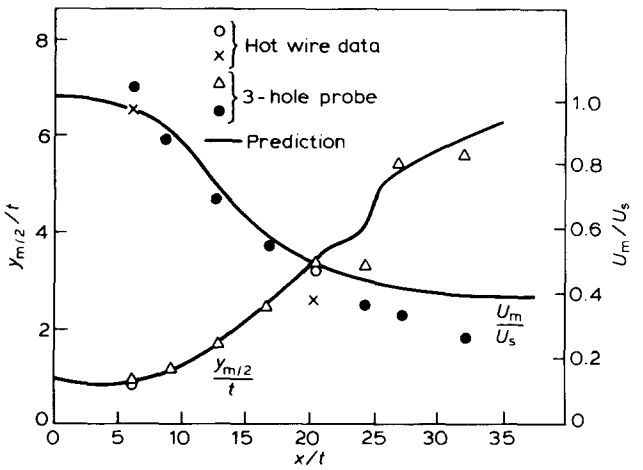

Fig 11 Case 7: growth/velocity decay

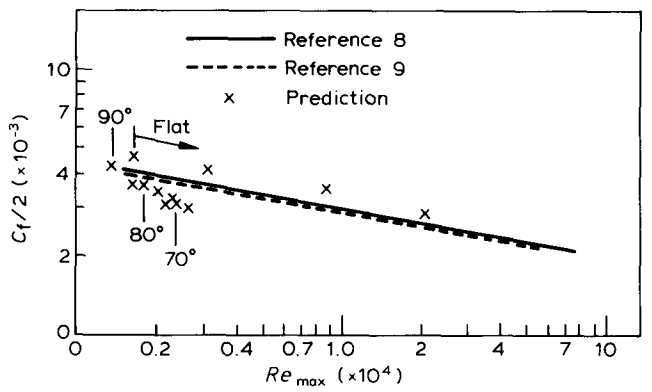

Fig 12 Case 6: wall shear stress

shows the maximum velocity decay which is poorly predicted. It appears that there is a problem with the initial development of the jet, which in this case is relatively thick. Fig 11 shows the growth rate and velocity decay for the thinner jet (Case 7). The velocity decay is predicted well, as is the growth rate.

For Case 6, Fig 12 shows the wall shear stress plotted against the Reynolds number based on maximum velocity and the distance from the wall at which it occurs. The predictions are compared with the law given by Bradshaw and Gee[8]. The predicted shear stress shows two regions: a decreasing Reynolds number up to the 90° position followed by an increasing Reynolds number thereafter. The agreement shows that Townsend's modified law of the wall is fairly satisfactory. This was ensured by keeping node 2, adjacent to the wall, inside the log-region. The mean velocity profiles are shown in Fig 13. At 50° the velocity profile (compared with measurements at 60°) is still developing and at 100° the tendency of the method to predict a too narrow velocity peak too close to the wall is noticeable. The shear stresses are generally under-predicted, particularly in the outer part of the jet (Fig 14). However, there the scatter in the experimental data indicates some uncertainty because the turbulence level is very high. The uneven values at 50° are associated with the development of the velocity profile and the positions of the mixing region boundaries.

Discussion

In general the partially parabolic calculation technique seems to work satisfactorily. There are some problems, particularly in the number and distribution of the grid points which affects the location of the 'mixing region' boundaries. The positions of the grid points are weighted towards the mean velocity maxima, consequently the positioning of y_3 and y_4 in Fig 2 is not always sufficiently accurate. This is the cause of the overestimates of shear stress at $\theta = 90°$ and 120° in Fig 9, and those of Fig 14.

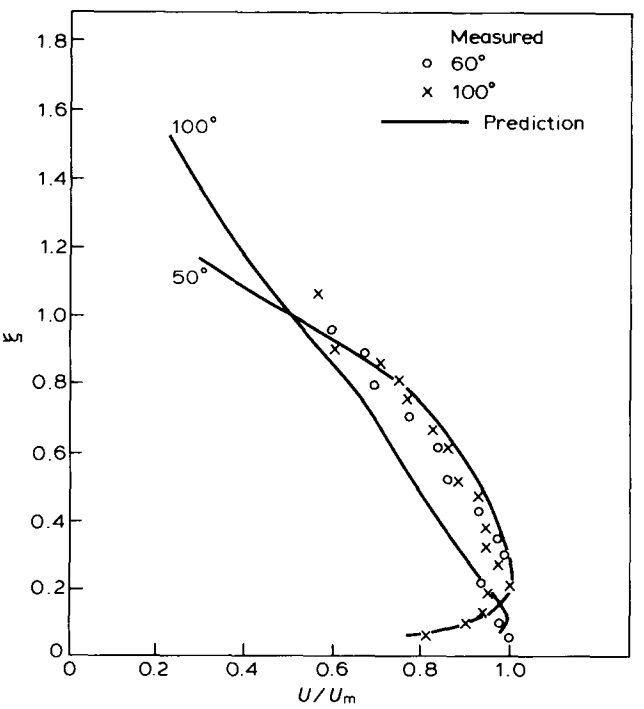

Fig 13 Case 6: velocity profiles

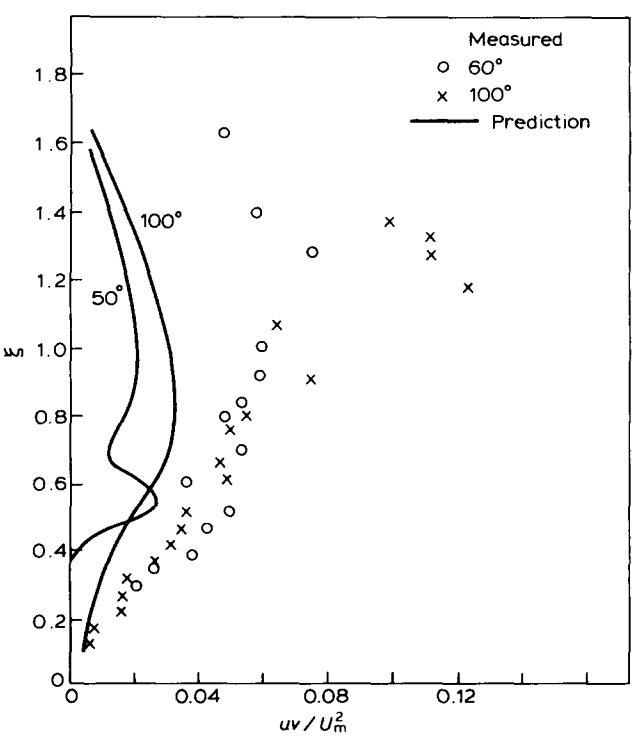

Fig 14 Case 6: shear stress profiles

These shear stress predictions highlight the somewhat arbitrary way of assigning the mixing length regions close to the wall as well.

In all the test cases with large streamwise curvature, U/U_m is underestimated near the velocity maxima. U is consequently overestimated near the jet edge. Consistent with this, the velocity decay rate is underestimated and V/U_m is predicted less than experimental data would indicate. For fully developed mean velocity profiles, the corresponding shear stress profiles are satisfactorily predicted near the mean velocity maxima. In regions of high lateral convection, where cross-stream transport by convection exceeds that due to diffusion, the diffusive terms are neglected and the convective terms are expressed in upwind difference form to ensure stability. This is a simplification of the combined difference scheme of Spalding[28] examined by Runchal[29]. The neglect of diffusion under these circumstances is particularly sensitive in regions of large $\partial U/\partial y$; hence the underestimation of U in the region of the U-maxima and the consequent underprediction of velocity decay rates.

The effect of the wall on the pressure-strain redistribution terms has been neglected for the turbulence modelling, where Irwin and Smith[21] have retained these extra terms. Their neglect is commensurate with that of the transport terms. This is an increasing source of error in the shear stress predictions in the sequence of Figs 5, 9 and 13. The profiles that show the best agreement are naturally those nearer the wall in Fig 5 in which there is a region of self-preservation. Despite neglecting the transport terms, the modelling procedure does predict the correct trend of the position of zero shear stress moving towards the wall with increasing curvature. Even so, an improved modelling technique would be a worthwhile development.

The comparison of the predictions for Cases 6 and 7 suffer due to the lack of two-dimensionality of the experimental data. Morrison[17] found significant evidence of three-dimensionality, notably base-plate boundary layer development and some unsteady spanwise periodicity of the flow.

The normal stress terms are modelled by simple proportionality to the shear stress, and are assumed isotropic. No correction was made for the preferential effect of streamline curvature on $\overline{v^2}$. The stability of the algorithm is sensitive to the crudity of the modelling for $\overline{v^2}$ via Eq (2) used to calculate the static pressure.

For the large streamline curvature, successful use is made of the iterative partial-parabolic procedure. The algorithm is unconditionally stable, provided upwind differences are used in the cross-stream direction for cases where lateral convection is high. This allows fairly large steps, of order $y_{m/2}$, to be taken around the surface and leads to an efficient computer calculation technique; the number of iterations required never exceeded five, typical run times were 5 s of cpu time (IBM 370) for the flare geometry with 30 cross-stream nodes. The corrections applied to the mixing length to allow for the extra rates of strain give basically satisfactory results. The simple addition for the flare geometry where both longitudinal curvature and divergence are present seems to give reasonable predictions of the mean features of the flow of engineering interest, eg growth rate. Only Cases 6 and 7 present problems in the region in which there is a sudden change in surface curvature ($dr/dx \rightarrow \infty$). It appears that the velocity decay is less well predicted as the ratio t/r is increased, as shown by Figs 10 and 11 for Cases 6 and 7.

As discussed by Morrison[17], the experimental results show that the change from the curved to conical section of the flare produces interesting effects. The present calculation method does not account for history effects except indirectly where the upstream mean velocity and hence shear stress profiles are affected by changes in pressure one grid station downstream on the previous iteration.

Conclusions

A calculation method for jet flows over curved surfaces has been developed. Successful use is made of the partially-parabolic technique with uncoupling of the streamwise and cross-stream momentum equations, leading to an efficient computer program allowing relatively large steps in the streamwise direction with only a few iterations.

The turbulence modelling of the extra rates of strain due to streamwise curvature and divergence is achieved by modifications to a mixing length model. The effects of the two rates of strain have been assumed to be additive, which gives reasonable results for the main features of the flow. The method is applicable generally to unconfined two-dimensional or axisymmetric jet flows with or without a solid boundary or curvature.

Areas for future development include the use of a stress transport type of turbulence model, which should not be too difficult to incorporate into the calculation method. Extension to compressible subsonic flow, and even to flows with supersonic patches, would be desirable since many practical applications have high blowing pressures.

Acknowledgement

The authors gratefully acknowledge the support of British Petroleum plc and the Science and Engineering Research Council for this work.

References

1. **Wilkins J., Witheridge R. E., Desty D. H., Mason J. T. M. and Newby N.** The design, development and performance of Indair and Mardair Flares. *9th Annual Offshore Technology Conference, Houston, Paper No. 2822, 1977*
2. **Newman B. G.** The deflexion of plane jets by adjacent boundaries – Coanda effect. *Boundary Layer and Flow Control (p 232), ed. Zachmann, G. V., Pergamon Press, 1961*
3. **Bradshaw P.** Effects of streamline curvature on turbulent flow. *AGARDograph No. 169, 1973*
4. **Glauert M. B.** The Wall Jet, *J. Fluid Mech.*, **1**, *1956, p 625*
5. **Schwarz W. H. and Cosart W. P.** Two-dimensional turbulent wall jet, *J. Fluid Mech.*, **10**, *1960, p 48*
6. **Myers G. E., Schauer J. J. and Eustis R. H.** Plane turbulent wall jet flow development and friction factor, *J. Basic Eng.*, **85**, *1963, p 47*
7. **Guitton D. E. and Newman B. G.** Self preserving turbulent wall jets over convex surfaces, *J. Fluid Mech.*, **81**, 1977, p 155
8. **Bradshaw P. and Gee M. T.** Turbulent wall jets with and without an external stream. *A.R.C., R & M 3252, 1960*
9. **Alcaraz E., Charnay G. and Mathieu J.** Measurements in a wall jet over a convex surface. *Phys. Fluids*, **20**, *1977, p 203*
10. **Wilson D. J. and Goldstein R. J.** Turbulent wall jets with cylindrical streamwise curvature. *J. Fluids Eng.*, **98**, *1976, p 550*

11. **Bakke P.** An experimental investigation of a wall jet, *J. Fluid Mech.*, **2**, *1957, p 467*

12. **Smits A. J., Eaton J. A. and Bradshaw P.** The response of a turbulent boundary layer to lateral divergence, *J. Fluid Mech.*, **94**, *1979, p 243*

13. **Sharma R. N.** Experimental investigation of conical wall jets, *A.I.A.A.*, **19**, *1981, p 28*

14. **Spalding D. B.** Genmix – a general computer program for two dimensional parabolic phenomena. *Science and Applications of Heat and Mass Transfer, Vol 1, Pergamon Press, 1977*

15. **Bradshaw P., Ferris D. H. and Atwell N. P.** Calculation of boundary layer development using the turbulent energy equation, *J. Fluid Mech.*, **28**, *1967, p 593*

16. **Cebeci T. and Smith A. M. O.** Analysis of turbulent boundry layers, *Academic Press, London, 1974*

17. **Morrison J. F.** A study of an axisymmetric wall jet with streamline curvature and its application to the Coanda Flare, *Ph.D. Thesis, Durham University, 1982*

18. **Patankar S. V. and Spalding D. B.** Heat and mass transfer in boundary layers, *Intertext books, London, 2nd ed, 1970*

19. **Patankar S. V. and Spalding D. B.** A calculation procedure for heat, mass and momentum transfer in three-dimensional parabolic flows, *Int. J. Heat Mass Transfer*, **15**, *1972, pp 1787*

20. **Townsend A. A.** Equilibrium layers and wall turbulence, *J. Fluid. Mech.*, **11**, *1961, p 97*

21. **Irwin H. P. A. and Smith P. A.** Prediction of the effect of streamline curvature on turbulence, *Phys. Fluid*, **18**, *1975, p 624*

22. **Launder B. E., Priddin C. H. and Sharma B. I.** The calculation of turbulent boundary layers on spinning and curved surfaces, *J. Fluids Eng.*, **99**, *1977, p 231*

23. **Gibson M. M. and Younis B. A.** Modelling the curved turbulent wall jet, *AIAA*, **20**, *1982, p 1707*

24. **So R. M. C. and Mellor G. L.** An experimental investigation of turbulent boundary layers along curved surfaces, *NASA CR1940, 1972*

25. **Bradshaw P.** The analogy between streamline curvature and buoyancy in turbulent shear flow, *J. Fluid Mech.*, **36**, *1969, p 177*

26. **So R. M. C.** Note on reference 10

27. **Rodi W.** A new method of analysing hot-wire signals in highly turbulent flow and its evaluation in a round jet. *DISA Information No 17, 1975, p 9*

28. **Spalding D. B.** A novel finite difference formulation for differential expressions involving both first and second derivatives, *Int. J. Numer. Meth. Eng.*, **4**, *1972, p 551*

29. **Runchal A. K.** Convergence and accuracy of three finite difference schemes for a two-dimensional conduction and convection problems, *Int. J. Numer. Meth. Eng.*, **4**, *1972, p 451*